HHS Public Access

Author manuscript

J Biomed Mater Res A. Author manuscript; available in PMC 2021 March 16.

Published in final edited form as:

J Biomed Mater Res A. 2016 August ; 104(8): 1922–1935. doi:10.1002/jbm.a.35726.

Development and characterization of a naturally derived lung extracellular matrix hydrogel

Robert A. Pouliot[1], **Patrick A. Link**[1], **Nabil S. Mikhaiel**[1], **Matthew B. Schneck**[1], **Michael S. Valentine**[1], **Franck J. Kamga Gninzeko**[1], **Joseph A. Herbert**[1], **Masahiro Sakagami**[2], **Rebecca L. Heise**[1,3]

[1]Department of Biomedical Engineering, Virginia Commonwealth University, Richmond, Virginia

[2]Department of Pharmaceutics, Virginia Commonwealth University, Richmond, Virginia

[3]Department of Physiology and Biophysics, Virginia Commonwealth University, Richmond, Virginia

Abstract

The complexity and rapid clearance mechanisms of lung tissue make it difficult to develop effective treatments for many chronic pathologies. We are investigating lung derived extracellular matrix (ECM) hydrogels as a novel approach for delivery of cellular therapies to the pulmonary system. The main objectives of this study include effective decellularization of porcine lung tissue, development of a hydrogel from the porcine ECM, and characterization of the material's composition, mechanical properties, and ability to support cellular growth. Our evaluation of the decellularized tissue indicated successful removal of cellular material and immunogenic remnants in the ECM. The self-assembly of the lung ECM hydrogel was rapid, reaching maximum modulus values within 3 min at 37°C. Rheological characterization showed the lung ECM hydrogel to have a concentration dependent storage modulus between 15 and 60 Pa. The purpose of this study was to evaluate our novel ECM derived hydrogel and measure its ability to support 3D culture of MSCs *in vitro* and *in vivo* delivery of MSCs. Our *in vitro* experiments using human mesenchymal stem cells demonstrated our novel ECM hydrogel's ability to enhance cellular attachment and viability. Our *in vivo* experiments demonstrated that rat MSC delivery in pre-gel solution significantly increased cell retention in the lung over 24 h in an emphysema rat model.

Keywords

decellularized lung; extracellular matrix; hydrogel; mesenchymal stem cells; rheometry

INTRODUCTION

Chronic lower respiratory diseases are the third leading cause of death in the US, resulting in almost 140,000 deaths in 2010.[1] Cell based therapies for treating chronic lung disease are often restricted by delivery obstacles inherent to pulmonary tissue. Unique challenges for the

Correspondence to: R. L. Heise; rlheise@vcu.edu.

Additional Supporting Information may be found in the online version of this article.

lung include: (1) the complex interweaving of airways, vasculature, and alveolar structures, (2) a volatile mechanical environment, and (3) multiple innate clearance mechanisms. Clearance mechanisms of the lung include the physical action of the mucociliary escalator, coughing, phagocytosis by alveolar macrophages, and absorption by the vasculature.[2] While aerosolization can be used to increase delivery efficiency of drugs and molecular factors to the lung,[3,4] this approach is limited by high shear forces. Thus, cell therapies are often delivered in solution by intratracheal injection.[5–7]

Mesenchymal stem cells (MSCs) are currently being used therapeutically to promote regeneration of damaged lung epithelial tissue through immune-modulation of the pulmonary microenvironment.[5,6] MSC therapies are thought to act through their influence over proinflammatory resident macrophages.[8–10]MSCs have been successfully delivered in solution as a therapy for acute lung injury in several models.[7,11–14] Despite their success these therapies have failed to produce significant improvement when addressing chronic lung pathologies due to the low retention in the tissue over time.[6,15] Cell delivery strategies for encapsulating and maintaining the therapeutic efficacy of the dosed cells have been developed from both natural and synthetic materials.[16–18] Inclusion of extracellular matrix (ECM) components in the cell delivery mechanism has been shown to help keep delivered cells in the tissue without negatively influencing the tissue environment. Recently a synthetic poly-L-lysine/ECM (fibrin) hydrogel was used to deliver lung derived MSCs in a sheep emphysema model. These hydrogels increased cell retention and resulted in better outcomes for the animals subjects.[19] In a similar strategy, we have developed a tissue specific ECM hydrogel derived from porcine lung tissue, which could be used to deliver and shield inoculated cells from the clearance mechanisms of the lung.

Tissue derived ECM is the next logical source to produce materials for organ transplant, tissue replacement, and novel tissue engineering approaches to cell and drug delivery.[20–26] Decellularized scaffolds are easily subjected to degradation and remodeling, and encourage macrophages to adopt the anti-inflammatory M2-like macrophage phenotype.[27–29] The organization, architecture, and composition of ECM components are tissue specific.[30] Lung derived ECM hydrogels retain native lung proteins, glycosaminoglycans (GAGs), and glycoproteins that pulmonary cells can recognize and remodel. These material components can also sequester and present bioactive molecules and tissue specific growth factors important in guiding cell behavior including migration, proliferation, differentiation, attachment, and signaling.[31]

ECM hydrogels have been developed from an increasing number of tissues, including: cardiac, epidermal, bladder, articular cartilage, nerve, and adipose sources.[32–37] These materials exhibit “injectability,” a unique property based on their gelation behavior. The ECM pre-gel solution is liquid at room temperature, but undergoes rapid self-assembly as the temperature approaches 37°C. This property allows the material to fill an area or settle into a defect just prior to gelation, encapsulating any cells or drugs delivered in the solution. *In vitro* studies have determined that several cell types exhibit a positive response to hydrogels derived from tissue specific sources including CNS[37] derived ECM and cardiac ventricular[22] derived ECM hydrogels. Recently, cardiac tissue derived ECM hydrogels have been shown to increase migration of endogenous cells into the damaged tissue when

delivered in an infarct model.[32] Naturally derived gels, which retain a significant portion of sulfated GAGs, can effectively bind and deliver heparin binding growth factors *in vivo*.[38] A lung derived ECM hydrogel could be an effective material for delivery and encapsulation of cells, drugs, or molecular factors at difficult to reach sites in lung disease models where epithelial cell and ECM defects at injury sites are observed.

This research project developed and characterized a novel porcine lung derived ECM hydrogel. We have investigated the outcomes of the decellularization process, effects on matrix organization, and described the structure, behavior, and mechanical properties of the resultant material. The goal of this study is to investigate the feasibility of our lung ECM hydrogel as a material for three dimensional cell culture *in vitro* and as cell delivery vehicle *in vivo*.

METHODS

Porcine lung tissue

Lung tissue was donated from slaughterhouse animals by Smithfield-Farmland. The lungs, heart, and trachea were isolated *en bloc* from a 6 month old pig at the facility, packed in ice, and delivered overnight in a sealed insulated container. Upon arrival, the heart was carefully removed to preserve the pulmonary artery for cannulation. Connective tissues surrounding the trachea, bronchi, and pulmonary artery were carefully excised to expose the vascular and airway structures necessary for perfusion. The right lung was removed at the main bronchus and the vasculature was dissected. The vasculature and airways previously connected to the right lung were then clamped or sutured shut to create a closed system for perfusion decellularization of the left lung. Both the trachea and pulmonary artery were sutured with tubing to streamline tissue perfusion.

Decellularization

Tissue decellularization was adapted from a protocol for C57BL/6 mice[39] and uses a similar reagent approach to previously published protocols for porcine and human lung by Price *et al*.[40] and Wagner *et al*.[41] Briefly, the lung was perfused three times with sterile filtered water with 1× penicillin/streptomycin (Life Technologies) though the trachea and vasculature. Between every rinse, the solution was removed passively, driven by the elasticity of the tissue. After rinsing the tissue, 1 L 0.1% Triton X-100 (Fisher Sci) was injected through the pulmonary vasculature and 1.5 L was injected into the airways through the trachea. Treated tissue was submerged in the same solution and incubated for 24 h at 4°C. Following incubation, the tissue was again rinsed three times with sterile filtered water to remove the chemical solution and all cellular debris. Tissue was then perfused again using a 2% sodium deoxycholate (Sigma) and incubated for an additional 24 h. On day three, tissue was rinsed and a DNase solution was pumped into the tissue, incubated for 60 min, and rinsed. A sodium chloride (Fisher Sci) solution was administered for an additional 60 min. Following the decellularization the tissue was rinsed with water three more times before being rinsed with sterile 1× Phosphate Buffered Saline (PBS) five times to remove as much decellularization agents and loose debris as possible. Decellularized tissue was sectioned and all discernable cartilaginous airways were removed before storage at −80°C.

Tissue histology

A minimum of three representative samples were taken from distal areas of both intact and decellularized lung, paraffin embedded, sectioned, and mounted. The slides were subsequently deparaffinized in xylenes and hydrated from 100% ethanol using stepwise rinses with increasing water to ethanol ratio. One set of lung sections were stained with hematoxylin and eosin (H&E) to confirm decellularization, and additional slides were stained using the ACCUSTAIN elastic stain kit (Sigma) to compare elastin and collagen organization before and after decellularization. A final set of slides was exposed overnight to 1:5 dilution of mouse α-Galactosidase primary antibody (Enzo), then washed and incubated with mouse SignalStain Boost Detection Reagent and stained with DAB chromogen solution (Cell Signaling) for 5 min. Stained slides were rinsed, dehydrated with xylenes, and mounted using Permount mounting medium (Fisher) prior to imaging using an Olympus IX71 Microscope (Olympus).

Picogreen double stranded DNA quantification

The DNA content of native and decellularized tissues was completed using the Quant-iT PicoGreen dsDNA assay kit. Briefly, intact and decellularized porcine lung tissues were sectioned into 100 mg samples and then diced using a razor blade. Each sample ($n = 3$ per tissue) was digested in 1 mL of papain digestion solution at 60°C overnight. The next day the samples were lightly centrifuged and diluted in 1× TE buffer for the following dilutions: 1:1, 1:4, 1:9, 1:19, 1:29, 1:49, 1:79, 1:99 and added to a solid black 96 well plate in 100 μL volumes in triplicate. A dsDNA standard was also prepared in the following (μg/mL) concentrations: 2, 1, 0.5, 0.25, 0.125, 0.0625, 0.03125, and 0. Picogreen reagent was then added to samples and standards and incubated in the dark at room temperature for 3 min. The samples were quantified in using a fluorescent plate reader with an excitation wavelength of 480 nm and emission wavelength of 520 nm.

Quantification of matrix components

Elastin/collagen quantification.—Both elastin and collagen quantification were completed using a protocol from Long and Tranquillo.[42] Collagen quantification was performed using a hydroxyproline assay. Elastin quantification was performed using the ninhydrin assay. Briefly, 50 mg samples were taken from both intact and decellularized porcine lung tissue and solubilized in 0.1*M* NaOH at 98°C for 45 min. Samples were then centrifuged (3000 g, 10 min), and the soluble proteins in the supernatant were removed, frozen, and lyophilized. Both the remaining insoluble elastin pellet and the lyophilized soluble proteins from the supernatant were hydrolyzed for 24 h in 6*M* HCl at 110°C. These hydrolyzed solutions were lyophilized and then diluted in 2 mL of DI water. The insoluble elastin samples were quantified using a ninhydrin assay and the collagen from the soluble protein samples was quantified using a hydroxyproline assay (Sigma).

Glycaosamnioglycan (GAG) quantification.—Sulfated GAGs were quantified using an alcian blue colorimetric assay described in Frazier *et al.*[43] Initially, 100 mg sections of both intact and decellularized tissue was diced and incubated at 4°C in a 4M guanidine HCL solubilization buffer (with 0.05*M* NA-Acetate and 2% w/v Triton x-100) for 12 h. An initial

dilution of dye test reagent was made with 100 mg of 8Gs Alcian blue powder (Sigma) in 10 mL of 0.018*M* H_2SO_4. This initial solution was diluted to a working solution 1/100 in 0.018*M* H_2SO_4 and Triton X-100 was added so that the final solution had 0.25%. The final solution was centrifuged at 10,000 g to remove any insoluble dye particles. Two hundred microliters of the solubilized tissue samples was added to 300 μL of the final dye solution and rigorously vortexed. These tubes were centrifuged (16,000 g, 10 min) at 4°C and then the resulting stained GAG pellet was isolated and dissolved in 500 μL of 8*M* guanidine HCL solution. Three hundred microliters of each sample was transferred to a 96 well plate and absorbance was measured at 600 nm using a Biotek plate reader.

Preparation of porcine lung derived ECM hydrogels

Processing and digestion of the decellularized scaffold into a pre-gel solution were adapted from a protocol for urinary bladder matrix.[36] Frozen tissue sections were lyophilized using a Flexi-Dry Lyophalizer (FTS Systems) and then milled using a SPEX model 6700 freezer mill. ECM powder was digested in a 0.01*M* HCl solution with pepsin from porcine gastric mucosa (Sigma-Aldrich) to solubilize the ECM components. ECM digestions were run for 48 h under constant agitation and ended using a 0.1*M* NaOH and a 10× PBS solutions bringing the pregel solution pH to 7.4 (+/−0.2) and PBS concentration to 1×. The pregel solution will self-assemble into a hydrogel at these conditions when incubated at 37°C.

SDS-PAGE protein size

Protein lysates were prepared for SDS page from intact porcine lung tissue, decellularized ECM powder, and ECM pregel solution (pepsin digested powder) using a 25 m*M*/ 1%SDS/ 4.5*M* Urea solubilization buffer and heating at 60° for 1 h. Lysates were centrifuged (12,000 g, 10 min) at 4°C and supernatants were sampled for soluble protein levels using a Bicinchoninic Acid (BCA) protein assay (Pierce). BCA values were used to balance protein levels by dilution; 25 μL of each balanced sample was added to 2× Laemmli buffer (Biorad) with 5% 2-mercaptoethanol (Fisher) and heated to 100°C for 5 min. Samples were cooled on an ice block before being loaded into an Any-kd Mini-Protean TGX Stain-Free Gel (Biorad) and run. Stain free gels were activated for 45 s and imaged using a ChemiDoc Touch imaging system (Biorad).

Scanning electron microscopy (SEM) imaging and histology

ECM hydrogels were formed from pregel solution incubated for 30 min before being fixed in glutaraldehyde. After fixation, the gels were sectioned and removed from the well using a biopsy punch. Lung tissue slices for imaging were isolated from both intact and decellularized porcine lung tissue and fixed in 4% paraformaldehyde for 48 h. Samples fixed for SEM imaging were rinsed in PBS and then incubated in 4% osmium tetroxide for an additional hour. After several washes tissue and gel samples were transferred from PBS to an ethanol solution using serial dilutions of ethanol from 25 to 100% incubating for up to 10 min between steps. Samples were then critical point dried using an autosamdri-814 critical point dryer (Tousimis) and mounted using conductive adhesive tabs (TED PELLA) for imaging. Samples were plasma sputter coated before imaging with a SEM (JEOL 6330F).

SEM images of decellularized tissue and ECM hydrogels were captured to characterize average fiber diameter and organizational patterns. The average diameter was determined by measuring the width of the fiber in three locations with approximately equal distribution along the fiber or fiber bundle using Matlab. For the tissue samples, a threshold of 300 nm was used to separate fibrils from more organized fiber bundles.

Rheometry

Rheometery was used to assess the mechanical properties of the hydrogels. Gel rheometry was completed using an ARG2 rheometer (TA Instruments) with 20 mm parallel plate geometry. ECM digests were completed <1 day prior to mechanical testing. An amplitude sweep was conducted for both 8 and 4 mg/mL ECM hydrogels to find an acceptable strain range for the experiment. To test the hydrogels 100 μL of the pregel solution was loaded onto the Peltier plate set at 4°C. The gap distance was then truncated to 300 to enclose the solution between the plate and the geometry. The temperature of the plate was increased from 4 to 37C° at 5°C/min and then held constant for 15 min. The oscillatory modulus of the sample was monitored continuously at a constant 0.1 Hz with a strain of 0.5% during the experiment. Samples were subjected to an oscillatory strain, developing a sinusoidal stress, G*, which represents the frequency dependent complex modulus. From G^*, G', and G'' were determined; where G' is the real part of the complex modulus, the storage modulus, and G'' is the imaginary portion of the complex modulus, the loss modulus.

Passive protein release

An *in vitro* assay was performed to determine the amount of protein that is passively released from the gel following complete gelation. In a 96-well TC plate, 100 μL of ECM pregel solution was incubated at 37°C for 1 h then gently washed with 200 μL 1× PBS, which was collected and replaced. PBS was collected from replicate wells at predetermined time points and stored for a BCA protein assay (Pierce) to determine the amount of protein released from the gel over time. Absorbance values were measured at 562 nm and converted to protein concentration (μg/mL) using values from the protein standard. Data is presented as total protein (μg) in each sample volume.

In vitro cell culture

All *in vitro* cell studies were completed using human bone marrow derived mesenchymal stem cells (hMSCs) obtained from Rooster Bio. Cells were defrosted and expanded in culture in enriched basal medium (RoosterBio) which was changed every 2–3 days. When cells were 80–90% confluent they were trypsinized, counted, and plated for attachment and encapsulation experiments. Cells used for these experiments were from the first three passages and quantification experiments were performed using a Quant-iT™ PicoGreen® dsDNA Assay Kit (Life Technologies). Background levels of dsDNA sequestered in the ECM material were normalized for using non-cell controls for protein coatings and gel encapsulation. These background values were subtracted so that only dsDNA from cultured cells is represented in the data.

Encapsulated cell viability

Viability of hMSCs encapsulated in formed ECM hydrogels was evaluated over 48 h. hMSCs were suspended at $3*10^4$ (cells/gel) in pregel solution at four concentrations: 2, 4, 6, and 8 mg/mL. The solutions were plated into 96 well plates in triplicate and incubated at 37°C for 30 min to form 500 mm thick hydrogels. Following gelation, 100 μL of media was carefully added to each well. After 2 days, the media was aspirated and samples were digested in papain digestion solution overnight at 65°C. Dole stranded DNA was quantified using a picogreen assay as previously described.

Encapsulated hMSC live/dead staining

A Live/Dead viability kit (Invitrogen) was used to visualize the performance of encapsulated hMSCs over time. In a 96 well clear, TC plate hMSCs were encapsulated in pregel solution at a density of 10,000 cells/well. The plate was incubated for 30 min to form 500 μm thick hydrogels and 100 μL of hMSC media was added to each well. The Live/Dead staining components were defrosted and added to 1× PBS to make a solution with 2 μ*M* calcien AM (green, Live) and 4 μ*M* EthD-1 (red, Dead). The media was first aspirated and 100 μL of Live/Dead staining solution was added to each well and incubated at room temperature for 30 min. The plate was then imaged using an Olympus IX71 Microscope using fluorescent light source and FITC (~490 nm, Live) and TRITC (~530 nm, Dead) filters. Images taken using each filter were colored and merged using FIJI to create Live/Dead composite images. Image quantification and cell counting was performed with NIH Image J on a minimum of 3 fields per sample.

Gene expression of encapsulated hMSCs

Gene Expression was performed using a CFX Connect realtime PCR machine (Biorad) to determine gene expression changes in MSCs when encapsulated in ECM hydrogels. hMSCs (~100 k cells/well) were either encapsulated in 300 μL ECM hydrogels or seeded onto TC plastic in 6 well plates. At 3 and 7-day time points RNA was collected and purified using a Qiagen RNeasy kit. RNA concentrations were balanced using nuclease free water and converted to cDNA using a high capacity cDNA reverse transcription kit (Applied Biosystems). Following conversion, the cDNA was probed using primers for Thy1, Sox2, and Oct4, with 18s as a housekeeping gene using SybrGreen (Applied Biosystems). Fold change for each experimental group is reported in reference to the 3-day plate control.

In vivo studies

To examine whether the lung ECM hydrogels enable initial lung delivery and retention of MSCs following administration intracheally, a feasibility study was performed in a rat model of emphysema. Emphysema was induced in male Sprague-Dawley rats weighing 250–300 g with an orotracheal solution spray instillation (0.2 mL) of porcine pancreatic elastase (PPE, Elastin Products) at 240 U/kg. On day 21, an impaired cardiopulmonary functionality was confirmed with a reduced exercise endurance on the treadmill according to the training and testing protocol established previously in-house.[44] Like our previous study,[45] emphysematous rats ran for only 9.85 ± 5.04 min in average, compared with 47.6 ± 3.8 min in healthy animals. On day 22, rats received an orotracheal solution instillation (0.1 mL) of 1

× 10^6 rat GFP-labeled bone-marrow derived MSCs (passage 3–5; Cyagen) with or without 4 mg/mL pregel porcine lung ECM hydrogel solution. At 24 h, rats were euthanized by exsanguination under sodium pentobarbital (i.p.;. 50 mg/kg), and lungs were inflated with 4% low-melting point agarose solution introduced at 20 cmH_2O hydrostatic pressure. After placing in ice for 5 min, the lungs were fixed with 10% formalin, paraffin embedded, sectioned to 5 μm thick slices, and mounted on slides. For visualization of the rat GFP positive MSCs, rat lung sections were deparaffinized in xylenes and rehydrated in a series of graded ethanol. Following blocking with 5% goat serum (Cell signaling), the slides were incubated for overnight at 4°C with a rabbit antibody to GFP (1:100; SC-8334 Santa Cruz;), followed by another 1 h incubation with Alexa Fluor 594-conjugated anti-rabbit antibody (1:1000; FisherSci) at room temperature. The slides were mounted in a Prolong Gold Antifade reagent with DAPI (ThemoFisher) and imaged on Olympus fluorescent microscope. Counts of GFP positive cells were performed using NIH Image J. Ten field images were taken per rat and three rats were used per treatment group. Another set of slides from each rat was stained with a TACS® 2 TdT-DAB *In Situ* Apoptosis Detection Kit according to the manufacturer's instructions (Trevigen).

Myloperoxidase assay

Myeloperoxidase (MPO) activity in each group of animals was quantified as a measure of lung tissue neutrophil accumulation using an approach developed by Goldblum *et al.*[46] and modified by Saluja *et al.*[44] The groups included healthy animals, positive elastase control, elastase treated animals dosed with rMSCs only, and elastase animals dosed with rMSCs in ECM pre-gel solution. Briefly, 100 mg of rat lung tissue was homogenized in 0.5 mL 0.02M EDTA (pH4.7) and brought to 0.75 mL with additional EDTA. After centrifugation (12,000 g, 15 min) at 4°C the supernatant was discarded and the tissue was re-homogenized in 0.5 mL in 0.5% hexadecyltrimethyl ammonium bromide (HTAB). After another centrifugation (12,000 g, 15 min) at 4°C, the supernatant was collected and saved. 10 μL of each supernatant was added to a 96 well plate in triplicate and 190 μL of test solution (0.17 mg/mL O-dianisidine dihydrochloride and 0.0005% H_2O_2) was added to the wells. Immediately after adding the test buffer the plate was read using a Biotek Synergy 2 plate reader at an absorbance of 405 nm every minute for 5 min. The change in absorbance was normalized with the BCA protein levels found in each supernatant, data is reported as $\Delta ABS_{5\ min}$/μg protein.

Statistical analysis

All quantitative hydrogel characterization and in vitro experimental studies were performed with a minimum of $n = 3$ in triplicate. *In vivo* treatment studies were performed with $n = 3$ rats per treatment group. Statistics were performed on each experimental measure with multiple groups with one-way ANOVA with Tukey tests for pair wise comparisons. When only comparing 2 groups, 2-tailed student's t-tests were performed. p values of <0.05 were considered significant, $*p < 0.05$, $**p < 0.01$, $***p < 0.001$ as indicated in the figure legends. We used GraphPad Prism 5 statistical analysis software.

RESULTS

Intact vs. decellularized lung tissue

An investigation of the porcine lung tissue before and after decellularization was completed using histology, immunohistochemistry, SEM, dsDNA quantification, and evaluation of key matrix components to determine the extent of decellularization and to describe the disruptive effects of detergents on the organization of matrix proteins. Slides from intact and decellularized tissue were stained using hemotoxylin and eosin to illustrate the removal of nuclei and most nuclear remnants from the remaining matrix [Fig. 1(A)]. Staining showed a depletion of the immunogenic membrane epitope, α-galactosidase, and is an indicator for the removal of cellular remnants from the matrix [Fig. 1(B)]. Picogreen quantification shows that dsDNA was reduced from 1,239.4 (+/− 62.7) [ng dsDNA/mg Tissue] to 57.4 (+/− 3.52) [ng dsDNA/mg Tissue] as a result of decellularization [Fig. 1(C)].

A qualitative study comparing intact mouse lung tissue slices to decellularized lung tissue slices shows that the decellularization process preserves many of the structures of the lung. Conserved feature structures include airways, alveolar spaces, and vasculature (Fig. 2). Histologic sections stained with Accustain Elastic stain show that elastic fibers are present in the tissue following decellularization but are depleted and much less organized [Fig 2(A–C,J–L)].

Quantification of matrix components

Decellularization using detergents is known to reduce the amounts of matrix proteins in the remaining scaffold. We quantified the changes in elastin, collagen, and sulfated GAGs and found that there was a significant decrease in all three. Absorbance data was collected for each colorimetric assay and normalized by the intact sample values to show the relative amount that each component is depleted during the decellularization process [Fig. 3(A)].

SDS-PAGE

Protein lysates from intact tissue, decellularized tissue powder, and pepsin digested ECM pre-gel solution were run on a wide band SDS-PAGE gel to separate proteins by size [Fig. 3(B)]. Intact tissue has the most bands as it includes both extracellular and intracellular matrix proteins. Decellularized matrix powder also has a significant number of distinct bands representing the spectrum of remaining ECM proteins following decellularization and processing. Pepsin is a fairly nonspecific protein enzyme and will act between any two unshielded amino acids responsible for the SDS-PAGE size distribution. Most of the largest proteins have been segmented and represented in the smaller bands. The nonspecific nature of pepsin also leads to a “smear” of protein sizes outside of the clear banding.

Fiber size and organization

While the ECM hydrogel lacks the highly organized matrix formations of collagen bundles seen in the decellularized tissue, it does have comparable fiber size to those found in the tissue. SEM imaging was used to evaluate ECM fibrils and fiber bundles in the hydrogel and in the tissue [Fig. 4(A–C)]. Measurement of fibrils found in the decellularized tissue and in the fixed hydrogels (<300 nm) found no significant difference between the groups, 138.03 ±

25.96 nm (tissue) and 87.104 ± 13.77 nm (hydrogels). The more organized fiber bundles (>300 nm), found only in the decellularized tissue sections, were determined to have an average thickness of 974.97 ± 81.33 nm, and were significantly different from both of the fibril groups.

Rheometry

A preliminary amplitude sweep was conducted to determine the acceptable strain range to test our material within the linear viscoelastic region (Supporting Information Fig. S1). This range was found to be between 0.1 and 1% strain for our samples; 0.5% was used for the experiments. The rheological properties of pig lung ECM hydrogels at 8 and 4 (mg/ mL) were examined during a temperature ramp and both the storage modulus (G') and loss modulus (G'') were found to increase as the pregel liquid solution self-assembled into a gel [Fig. 5(A,B)]. Results were compared with ECM hydrogels derived from other tissues (Table I). The measurements taken during a temperature ramp 4 to 37°C at 3°C increments show that the self-assembly mechanism of the pre-gel solution start around 35°C and that the majority of the mechanical change related to the gelation occur shortly after the gel reaches physiologic body temperature of 37°C. The strain used to test the hydrogels was found to have a significant impact on the results. Rheometry experiments conducted using 5% strain resulted in irreversible deformation of the ECM hydrogels at 8 and 4 (mg/mL) and significantly lower modulus values as the temperature was ramped to induce gelation (Supporting Information Fig. S1). Testing on similar materials derived from other sources used a range of testing conditions, including different strains, which could be partially responsible for the large spectrum of mechanical properties amongst published results (Table I).

Passive protein release

Proteins passively released from the material could have a significant effect in addition to the actual degradation products of the hydrogel *in vivo*. During our investigation, we found that there is a significant amount of nonsoluble or non-assembled protein that is initially trapped during gelation but quickly released into the milieu. Using 1× PBS to collect these proteins over time we determined that measureable passive protein loss occurs over 14 days, with the maximum protein release occurring within the first 48 h after gelation [Fig. 6(A)]. Comparison of hydrogels directly following gelation and after 14 days of protein release using SEM yields an observable difference in the quantity and organization of proteins in the hydrogel network [Fig. 6(B)] There was also a visual difference in the density of nonintegrated proteins from day 1 to day 14, which suggests that much of the measured protein release could have been diffusion from the hydrogel.

Encapsulation of hMSCs

hMSCs encapsulated in lung derived ECM hydrogels were found to maintain viability at higher levels than encapsulation in a commercially available collagen hydrogel [Fig. 7(A)]. In addition to hMSC experiments using dsDNA quantification, cell viability was confirmed by staining encapsulated hMSCs grown in hydrogels using a Live/Dead staining kit. Quantification of these images showed that there are a significantly greater number of cells alive at the 5 days indicating active proliferation in the gel [Fig. 7(B)]. This is clearly

demonstrated visually in representative images taken from day 2 and day 5 [Fig. 7(C,D)], minimal dead cells were observed at either time point. In addition, cell attachment to and contraction of the hydrogels demonstrates their ability to recognize and use binding sites inherent in the matrix derived material.

Encapsulated MSC gene expression

In vitro gene expression analysis of MSCs grown within lung ECM hydrogels indicates that stem-ness markers are not lost during encapsulated culture (Fig. 8). Thy1 showed no significant change compared with cells grown on a tissue culture plate control. Sox2 and Oct4 expression were significantly increased compared to plate control on day 3, and the expression returned to plate control levels at Day 7.

In vivo delivery and inflammatory indicator

Delivery of rat MSCs intratracheally using the lung ECM hydrogel was determined to significantly increase the number of GFP positive cells in the tissue by nearly 2.5 times the amount after 24 h when compared with rat MSCs delivered in saline [Fig 9(A)]. Representative images from each group are shown in Figure 9(A,B) showing GFP tagged MSCs in the alveolar regions in the elastase treated rat lungs. MPO is a granular enzyme expressed by polymorphonuclear neutrophils and alveolar macrophages, catalyzing the synthesis of hypoclorous acid, a by-product of hydrogen peroxide and is indicative of inflammatory response. PPE induced emphysema is not expected to cause large amounts of MPO. Treatments of MSC and MSC+ ECM in the PPE treated rats did not significantly increase MPO activity compared with Saline in the PPE rats, indicating that the treatment at did not cause increased inflammation [Fig. 9(D)]. Apoptotic cells were not detected in the rat lung sections as shown by lack of dark brown staining in Figure 9(E,F).

DISCUSSION

The results of our study demonstrate that porcine lung tissue can be decellularized, processed, and digested to produce hydrogels derived from the native ECM components. These hydrogels exhibit unique self-assembly behavior, architecture, and mechanical properties credited to materials derived from other tissue sources. *In vitro* investigation has revealed that these hydrogels can conduct attachment, proliferation, and maintain viability of encapsulated cells.

The sodium deoxycholate/triton approach effectively decellularized porcine lung tissue and conserved many of the important structural components from the native ECM. Staining with hematoxylin and eosin confirmed that a large majority of the nuclear structures were removed and further quantification of total double stranded DNA indicates a 95.7% reduction after decellularization [Fig. 1(A,C)]. Evaluation of remnant nuclear structures or DNA in the scaffold is often used as a primary method for gauging effectiveness of the decellularization regimen used. Development of biomaterials from xenogenic sources is complicated by the presence of immunogenic antigens. One major consideration is the alpha gal epitope, which can result in an acute rejection response without prior depletion of the antigen.[45,47] The alpha gal antibody specifically recognizes the alpha-gal epitope found on

the cell surface in the majority of mammals with the exception of Old World monkeys, apes, and humans. In humans, a significant 1% of all circulating immunoglobulins are specific for the alpha-gal epitope, which can lead to catastrophic failure of xenogenic materials without depletion of the antigen.[48] Comparative DAB staining using a primary antibody for alpha galactosidase before and after decellularization suggests that cell remnants including matrix bound membrane sections, debris, and intracellular proteins were mostly removed and prevented from sequestration in the matrix [Fig. 1(B)].

Every approach for tissue decellularization influences the quantity and quality of ECM components retained in the acellular framework.[23,25,49] The resulting profile of depleted or damaged matrix proteins plays a major role in determining the ultimate physical properties of the hydrogel and its capacity for supporting cell-matrix interactions.[26,49,50] Comparison of the elastin and collagen organization in major lung structures pre and post decellularization (Fig. 2) hints at the disruptive nature of the deoxycholate/triton approach used.

Colorimetric assays confirmed a reduction of key matrix components during the decellularization process including elastin, collagen, and sulfated GAGs [Fig. 3(A)]. The assay also indicates that there are still robust amounts of these matrix components present in the decellularized matrix prior to pepsin digestion. The changes in the profile and size distribution of proteins resulting from decellularization, processing, and digestion are evident in the SDS-PAGE data presented in Figure 3(B). There are distinct matrix components input into the pepsin digestion. However, due to the unspecific cleavage it is difficult to determine the state of each of these components following digestion in the pregel. This unspecific cleavage of the pepsin digestion makes it difficult to apply traditional matrix quantification and mass spec approaches to the pregel solution.

The lyophalization, milling, and digestion to transform the acellular matrix into a hydrogel results in the reduction of highly organized ECM structures, bundles, and fibers into a less dense and more randomly organized material (Fig. 4). A quantification of fiber sizes revealed that the organized fiber bundles were much more prevalent in the decellularized tissue. The fibers measured in the hydrogel sample were much thinner with less variance suggesting that proteins from the tissue had been reduced to subunits during the digestion and then reassembled during gelation.

Solid tissue engineering scaffolds are appropriate for addressing tissue engineering needs in tissues with a static mechanical environment. They are, however, much less applicable in tissues that undergo complex deformation such as the heart or lungs. The deformability of hydrogels can prevent damage to the native tissue under strain while protecting encapsulated cells or drugs. The novel lung ECM hydrogels we have developed have mechanical properties comparable to similar scaffolds (Table I). In general, the shear modulus of soft tissues are significantly higher than what we have determined for lung derived hydrogels.[51] However, for a therapeutic delivery vehicle, the ability to maintain cells or drugs at target locations in the tissue is more important than a perfect match with native the tissue mechanics.

The gelation behavior of the hydrogel contributes to the practicality of the hydrogel system, especially for use in injectable delivery. We determined that our lung derived hydrogel shows little to no gelation activity until the temperature of the material exceeds 32°C, the pregel solution then completely self assembles in 3 min once the material reaches 37°C (Fig. 5). This can potentially allow drugs or cells to be delivered in an injectable liquid solution, encapsulating the payload once the solution reaches the target tissue. For an intratracheal delivery, the goal would be to deliver the pregel solution to the alveolar spaces before gelation to reduce the chances that airways are obstructed. Studies using ECM gels derived from other tissues suggest that the mechanical properties and gelation time can be directed by modifying the starting temperature, protein concentration, pH, or ion concentration,[31,52] which could be tailored using our model to ensure that the majority of the solution reaches the alveolar spaces before gelation.

A comparison of the published rheometry data for other tissue derived ECM hydrogels revealed a large variation in the experimental methods and conditions used. We have demonstrated that there is a significant difference in the modulus found using strains of 0.5 and 5%. We attribute this difference to the larger strain being outside of the linear viscoelastic (LVE) region as determined by an amplitude sweep. While 5% strain could be in the LVE region for some of the more robust materials derived from highly collagenous tissues such as bladder, dermis, and spinal cord, it is possible that such a large strain irreversibly damages hydrogel samples during the first rheometric measurements.

Degradation products of previously described ECM biomaterials have been found to have additional beneficial functions including antibacterial properties[53] and chemo attractant promoting cell taxis.[54] In this study, our analysis of the passive release profile of the hydrogel revealed that a large amount of protein can be collected in the wash immediately after complete gelation, and that the majority of protein release happens within the first 48 h [Fig. 6(A)]. This suggests that not all constituents of the pregel solution are involved in self-assembly of the hydrogel and that possibly not all of the isolated protein been solubilized with our current digestion protocol. While it is not clear that proteins passively released from a lung derived hydrogel are beneficial they have not been found to be cytotoxic in preliminary *in vitro* experiments or in the acute *in vivo* model.

The behavior of cell types grown on tissue specific ECM is a driving force behind proponents of tissue specific ECM for tissue engineering scaffold materials. Many whole organ decellularization studies have investigated the differentiation and organization of tissue progenitor cells in culture on whole organ scaffolds.[21,49,55,56] Decellularized whole organ materials have the advantage of mechanical properties closer to those of the native tissue, physical cues from intact tissue structures, as well as the biochemical cues of the ECM. All of these help guide seeded cells find their functional identity.

In vitro investigations with ECM derived materials have found that the materials are noncytotoxic,[34,37] promote migration of relevant cell types,[57] and are equal or better at maintaining cell viability when compared to control collagen hydrogels.[22,35] During our investigation we found that hMSCs encapsulated in lung ECM hydrogels remain viable at higher or comparable levels to those encapsulated in a commercially available collagen type

I hydrogel. We also observed that cells proliferate more in lower concentration ECM hydrogels, we believe that this difference is due to there being less support and encapsulation in the 4 and 2 mg/mL, and which may allow the cells to sink toward the bottom of the gels to sense the stiffness of the tissue culture plastic.

In addition to the activity and viability of cells encapsulated in ECM hydrogels we were interested in determining the effect of encapsulation on the genetic expression of hMSCs. We looked at Thy1 (CD90), which is a common MSC marker, and Sox2 and Oct4 which are prominent actors in the signaling pathways responsible for MSCs retaining their pluripotency and "stemness." Many of the therapeutic functions of MSCs come from their immunomodulatory functions, which would be minimized if encapsulation caused differentiation.

Significant increases in Sox2 and Oct4 suggest that the cells are responding as they attach and migrate through the hydrogel, but their return to plate control levels by day seven suggests that encapsulated MSCs maintain their original phenotype.

Finally, the *in vivo* feasibility study for intratracheal cell delivery in Figure 9 confirmed that the ECM hydrogel vehicle increased cell retention when compared to a nonvehicle control. In both groups, there are examples of the GFP antibody localizing to immune cells suggesting that some cells are phagocytosed regardless of delivery method. However, it is clear that there are more intact GFP-tagged cells when delivered in a pregel solution when compared with the non-vehicle control. Additionally, the absence of apoptotic cells as indicated by an apoptotic staining assay on serial sections used for quantification of dosed cells in the tissue suggests that the GFP tagged cells found in the tissue remain viable. Further investigation of the treated animal groups revealed that additional inflammation was not caused in the short term as evidenced by the MPO data; however, longer term studies will need to be performed to more extensively assess the pro- or anti-inflammatory effects of the hydrogel as a treatment. The successful encapsulation and maintenance of viable MSCs in a lung derived ECM hydrogel both *in vitro* and *in vivo* supports further investigation of this material for cell delivery purposes.

The research presented in this study has validated our decellularization and processing approach for developing a lung derived ECM hydrogel for regenerative medicine applications including cell delivery. The mechanical properties we measured show our hydrogel to be suitable for delivery into the mechanically dynamic tissues of the lung. The thermosensitive self-assembly behavior of our hydrogel can allow us to tailor delivery strategies to optimize delivery of the MSCs in a thin hydrogel layer in the alveoli. *In vitro* experiments determined that stem cells remain viable and can even proliferate once encapsulated. Additionally, the ECM components in our hydrogels may have retained many of their natural binding sites or sequestered cytokines, which may promote endogenous cell migration. It is important to understand the effect of our hydrogels on cell gene expression or ultimate fate and the effects of proteins released from the material. In the future, we will continue to look at cell – ECM interactions *in vitro*, in an effort to determine if encapsulated MSCs retain their ability to modulate a simulated pro-inflammatory environment, as well investigate other potential applications for the hydrogel vehicle itself.

CONCLUSION

The results of this study show that a lung derived ECM hydrogel may have value in regenerative medicine applications. We have successfully demonstrated that decellularized lung tissue can be processed and digested to create a smart material, which is liquid at room temperature, but undergoes self-assembly into a hydrogel as the environment approaches 37°C. During this study, we have thoroughly characterized the composition, structure, gelation kinetics, mechanical properties, and protein release behavior of the material. In addition we have conducted initial *in vitro* experiments which suggest MSCs remain viable and maintain their "stemness" during encapsulation in hydrogels for up to a week. Delivery of MSCs intratracheally in a rat model demonstrated that encapsulation of the cells in the hydrogel resulted in increased retention of the cells after 24 h. The results of this study support continued investigation of lung derived ECM hydrogels as a cell or drug delivery vehicle.

Supplementary Material

Refer to Web version on PubMed Central for supplementary material.

ACKNOWLEDGMENTS

Hydrogel and tissue samples were prepared for SEM at the VCU Department of Anatomy and Neurobiology Microscopy Facility supported, in part, by funding from NIH-NINDS Center Core Grant 5 P30 NS047463 and, in part, by funding form NIH-NCI Cancer Center Support Grant P30 CA016059. SEM imaging of samples at the VCU Nanotechnology Core Characterization Facility (NCC). The VCU Plastic Surgery department for use of their SPEX Freezer Mill. The Authors would like to acknowledge the following laboratories at VCU for use of equipment: Wen/Zhang Lab, Boyan, Schwartz, Olivares-Navarette Lab, and the Yang Lab. The authors would like to acknowledge Hua Li for her help with the animal work.

REFERENCES

1. Kochanek KD, Xu J, Murphy SL, Miniño AM, Kung HC. National vital statistics reports. Natl Vital Stat Rep 2011;59:1.
2. Olsson B, Bondesson E, Borgstrom L, Edsbacker S, Eirefelt S, Ekelund K, Gustavsson L, Hegelund-Myrback T. In Smyth HDC, Hickey AJ, editors. Controlled Pulmonary Drug Delivery. Ch.2: Pulmonary Drug Metabolism, Clearance, and Absorption. New York: Springer; 2011. p 21–50.
3. Labiris NR, Dolovich MB. Pulmonary drug delivery. Part I: Physiological factors affecting therapeutic effectiveness of aerosolized medications: Physiological factors affecting the effectiveness of inhaled drugs. Br J Clin Pharmacol 2003;56:588–599. [PubMed: 14616418]
4. Shah ND, Shah VV, Chivate ND. Pulmonary drug delivery: A promising approach. J Appl Pharm Sci 2012;2:33–37.
5. D'Agostino B, Sullo N, Siniscalco D, De Angelis A, Rossi F. Mesenchymal stem cell therapy for the treatment of chronic obstructive pulmonary disease. Expert Opin Biol Ther 2010;10:681–687. [PubMed: 20384521]
6. Weiss DJ, Casaburi R, Flannery R, LeRoux-Williams M, Tashkin DP. A placebo-controlled, randomized trial of mesenchymal stem cells in COPD mesenchymal stem cells for COPD. Chest J 2013; 143:1590–1598.
7. Wang D, Morales JE, Calame DG, Alcorn JL, Wetsel RA. Transplantation of human embryonic stem cell–derived alveolar epithelial type II cells abrogates acute lung injury in mice. Mol. Ther 2010;18:625–634. [PubMed: 20087316]
8. Prockop DJ, Youn Oh J. Mesenchymal stem/stromal cells (MSCs): Role as guardians of inflammation. Mol Ther 2012;20:14–20. [PubMed: 22008910]

9. Choi H, Lee RH, Bazhanov N, Oh JY, Prockop DJ. Anti-inflammatory protein TSG-6 secreted by activated MSCs attenuates zymosan-induced mouse peritonitis by decreasing TLR2/NF- B signaling in resident macrophages. Blood 2011;118:330–338. [PubMed: 21551236]
10. Oh JY, Roddy G, Choi H, Lee RH, Ylostalo J, Rosa R, Prockop D. Anti-inflammatory protein TSG-6 reduces inflammatory damage to the cornea following chemical and mechanical injury. Proc Natl Acad Sci USA 2010;107:16875–16880. [PubMed: 20837529]
11. Matthay MA, Goolaerts A, Howard JP, Woo Lee J. Mesenchymal stem cells for acute lung injury: Preclinical evidence. Crit Care Med 2010;38:S569–S573. [PubMed: 21164399]
12. Lee JW, Gupta N, Serikov V, Matthay MA. Potential application of mesenchymal stem cells in acute lung injury. Expert Opin Biol Ther 2009;9:1259–1270. [PubMed: 19691441]
13. Mei SH, McCarter S, Deng Y, Parker C, Liles C, Stewart D. Prevention of LPS-induced acute lung injury in mice by mesenchymal stem cells overexpressing angiopoietin 1. PLoS Med 2007;4:e269 [PubMed: 17803352]
14. Lee JW, Fang X, Gupta N, Serikov V, Matthay MA. Allogeneic human mesenchymal stem cells for treatment of E. coli endotoxin-induced acute lung injury in the ex vivo perfused human lung. Proc Natl Acad Sci USA 2009;106:16357–16362. [PubMed: 19721001]
15. Zhang WG, He L, Shi XM, Wu SS, Zhang B, Mei L, Xu YJ, Zhang ZX, Zhao JP, Zhang HL. Regulation of transplanted mesenchymal stem cells by the lung progenitor niche in rats with chronic obstructive pulmonary disease. Respir Res 2014;15:33 [PubMed: 24661402]
16. Stucky EC, Schloss RS, Yarmush ML, Shreiber DI. Alginate microencapsulation of mesenchymal stromal cells enhances modulation of the neuro-inflammatory response. Cytotherapy 2015;17: 1353–1364. [PubMed: 26210574]
17. Garate A, Tsai L, Murthy S, Tyagi S, Mazan M, Hoffman A. Assessment of the behavior of mesenchymal stem cells immobilized in biomimetic alginate microcapsules. Mol. Pharm 2015;12: 3953–3962. [PubMed: 26448513]
18. Lu S, Lee EJ, Lam J, Tabata Y, Mikos AG. Evaluation of Gelatin Microparticles as Adherent-Substrates for Mesenchymal Stem Cells in a Hydrogel Composite. Ann Biomed Eng. 2016. Epub ahead of print.
19. Ingenito EP. Autologous Lung-Derived Mesenchymal Stem Cell Transplantation in Experimental Emphysema. Cell Transplant 2012;21:175–189. [PubMed: 21294955]
20. Badylak S, Freytes D, Gilbert T. Extracellular matrix as a biological scaffold material: Structure and function. Acta Biomater 2009;5:1–13. [PubMed: 18938117]
21. Daly AB. Initial binding and recellularization of decellularized mouse lung scaffolds with bone marrow-derived mesenchymal stromal cells. Tissue Eng Part A 2012;18:1–16. [PubMed: 21756220]
22. French KM, Boopathy AV, DeQuach JA, Chingozha L, Lu H, Christman KL, Davis ME. A naturally derived cardiac extracellular matrix enhances cardiac progenitor cell behavior in vitro. Acta Biomater 2012;8:4357–4364. [PubMed: 22842035]
23. Gilbert T, Sellaro T, Badylak S. Decellularization of tissues and organs. Biomaterials. 2006;27:3675–3683. [PubMed: 16519932]
24. Hoshiba T, Lu H, Kawazoe N, Chen G. Decellularized matrices for tissue engineering. Expert Opin Biol Ther 2010;10:1717–1728. [PubMed: 21058932]
25. Nichols JE, Niles JA, Cortiella J. Production and utilization of acellular lung scaffolds in tissue engineering. J Cell Biochem 2012;113:2185–2192. [PubMed: 22573544]
26. Petersen TH, Calle EA, Colehour MB, Niklason LE. Matrix composition and mechanics of decellularized lung scaffolds. Cells Tissues Organs 2012;195:222–231. [PubMed: 21502745]
27. Badylak SF, Valentin JE, Ravindra AK, McCabe GP, Stewart-Akers AM. Macrophage Phenotype as a Determinant of Biologic Scaffold Remodeling. Tissue Eng Part A 2008;14:1835–1842. [PubMed: 18950271]
28. Badylak SF. The extracellular matrix as a biologic scaffold material*. Biomaterials 2007;28:3587–3593. [PubMed: 17524477]
29. Valentin JE, Badylak JS, McCabe GP, Badylak SF. Extracellular matrix bioscaffolds for orthopaedic applications. J Bone Joint Surg Am 2006;88:2673–2686. [PubMed: 17142418]

30. Bonvillain RW, Danchuk S, Sullivan DE, Betancourt AM, Semon JA, Eagle ME, Mayeux JP, Gregory AN, Wang G, Townley IK, Borg ZD, Weiss DJ, Bunnell BA. A Nonhuman Primate Model of Lung Regeneration: Detergent-Mediated Decellularization and Initial *In Vitro* Recellularization with Mesenchymal Stem Cells. Tissue Eng Part A 2012;18:2437–2452. [PubMed: 22764775]

31. Johnson TD, Lin SY, Christman KL. Tailoring material properties of a nanofibrous extracellular matrix derived hydrogel. Nanotechnology 2011;22:494015 [PubMed: 22101810]

32. Singelyn JM, Sundaramurthy P, Johnson TD, Schup-Magoffin PJ, Hu DP, Faul DM, Wang J, Mayle KM, Bartels K, Salvatore M, Kinsey A, DeMaria AN, Dib N, Christman KL. Catheter-Deliverable Hydrogel Derived From Decellularized Ventricular Extracellular Matrix Increases Endogenous Cardiomyocytes and Preserves Cardiac Function Post-Myocardial Infarction. J Am Coll Cardiol 2012; 59:751–763. [PubMed: 22340268]

33. Kwon JS, Yoon SM, Shim SW, Park JH, Min KJ, Oh HJ, Kim JH, Kim YJ, Yoon JJ, Choi BH, Kim MS. Injectable extracellular matrix hydrogel developed using porcine articular cartilage. Int J Pharm 2013;454:183–191. [PubMed: 23834831]

34. Wolf MT. A hydrogel derived from decellularized dermal extracellular matrix. Biomaterials 2012;33:7028–7038. [PubMed: 22789723]

35. Young DA, Ibrahim DO, Hu D, Christman KL. Injectable hydrogel scaffold from decellularized human lipoaspirate. Acta Biomater 2011;7:1040–1049. [PubMed: 20932943]

36. Freytes DO, Martin J, Velankar SS, Lee AS, Badylak SF. Preparation and rheological characterization of a gel form of the porcine urinary bladder matrix. Biomaterials 2008;29:1630–1637. [PubMed: 18201760]

37. Medberry CJ, Crapo PM, Siu BF, Carruthers CA, Wolf MT, Nagarkar SP, Agrawal V, Jones KE, Kelly J, Johnson SA, Velankar SS, Watkins SC, Modo M, Badylak SF. Hydrogels derived from central nervous system extracellular matrix. Biomaterials 2013;34: 1033–1040. [PubMed: 23158935]

38. Seif-Naraghi SB, Horn D, Schup-Magoffin PJ, Christman KL. Injectable extracellular matrix derived hydrogel provides a platform for enhanced retention and delivery of a heparin-binding growth factor. Acta Biomater 2012;8:3695–3703. [PubMed: 22750737]

39. Price AP, England KA, Matson AM, Blazar BR, Panoskaltsis-Mortari A. Development of a decellularized lung bioreactor system for bioengineering the lung: The matrix reloaded. Tissue Eng Part A 2010;16:2581–2591. [PubMed: 20297903]

40. Price AP, Godin LM, Domek A, Cotter T, D'Cunha J, Taylor DA, Panoskaltsis-Mortari A. Automated decellularization of intact, human-sized lungs for tissue engineering. Tissue Eng Part C Methods. 2015;21:94–103. [PubMed: 24826875]

41. Wagner DE, Bonenfant NR, Parsons CS, Sokocevic D, Brooks EM, Borg ZD, Lathrop MJ, Wallis JD, Daly AB, Lam YW, Deng B, DeSarno MJ, Ashikaga T, Loi R, Weiss DJ. Comparative decellularization and recellularization of normal versus emphysematous human lungs. Biomaterials 2014;35:3281–3297. [PubMed: 24461327]

42. Long JL, Tranquillo RT. Elastic fiber production in cardiovascular tissue-equivalents. Matrix Biol 2003;22:339–350. [PubMed: 12935818]

43. Frazier SB, Roodhouse KA, Hourcade DE, Zhang L. The Quantification of Glycosaminoglycans: A Comparison of HPLC, Carbazole, and Alcian Blue Methods. Open Glycosci 2008;1:31–39. [PubMed: 20640171]

44. Saluja B, Li H, Desai UR, Voelkel NF, Sakagami M. Sulfated Caffeic Acid Dehydropolymer Attenuates Elastase and Cigarette Smoke Extract–induced Emphysema in Rats: Sustained Activity and a Need of Pulmonary Delivery. Lung 2014;192:481–492. [PubMed: 24831783]

45. Macher BA, Galili U. The Galα1,3Galβ1,4GlcNAc-R (α-Gal) epitope: A carbohydrate of unique evolution and clinical relevance. Biochim Biophys Acta 2008;1780:75–88. [PubMed: 18047841]

46. Goldblum SE, Wu KM, Jay M. Lung myeloperoxidase as a measure of pulmonary leukostasis in rabbits. J Appl Physiol 1985;59: 1978–1985. [PubMed: 3001018]

47. Badylak SF. Decellularized allogeneic and xenogeneic tissue as a bioscaffold for regenerative medicine: Factors that influence the host response. Ann Biomed Eng 2014;42:1517–1527. [PubMed: 24402648]

48. Naso F, Gandaglia A, Iop L, Spina M, Gerosa G. First quantitative assay of alpha-Gal in soft tissues: Presence and distribution of the epitope before and after cell removal from xenogeneic heart valves. Acta Biomater 2011;7:1728–1734. [PubMed: 21118731]

49. Wallis JM, Borg ZD, Daly AB, Deng B, Ballif BA, Allen GB, Jaworski DM, Weiss DJ. Comparative assessment of detergent-based protocols for mouse lung de-cellularization and re-cellularization. Tissue Eng Part C Methods 2012;18:420–432. [PubMed: 22165818]

50. Gilbert TW, Daly KA, Brennan-Pierce EP, Johnson SA, Carruthers CA, D'Amore A, Nagarkar SP, Velankar SS, Badylak SF. Strategies for tissue and organ decellularization. J Cell Biochem 2012;113: 2217–2222. [PubMed: 22415903]

51. Butcher DT, Alliston T, Weaver VM. A tense situation: forcing tumour progression. Nat Rev Cancer 2009;9:108–122. [PubMed: 19165226]

52. Singelyn JM, Christman KL. Modulation of Material Properties of a Decellularized Myocardial Matrix Scaffold. Macromol Biosci 2011;11:731–738. [PubMed: 21322109]

53. Brennan EP, Reing J, Chew D, Myers-Irvin JM, Young EJ, Badylak SF. Antibacterial Activity within Degradation Products of Biological Scaffolds Composed of Extracellular Matrix. Tissue Eng 2006; 12:2949–2955. [PubMed: 17518662]

54. Reing JE, Zhang L, Myers-Irvin J, Cordero KE, Freytes DO, Heber-Katz E, Bedelbaeva K, McIntosh D, Dewilde A, Braunhut SJ. Degradation products of extracellular matrix affect cell migration and proliferation. Tissue Eng Part A 2008;15:605–614.

55. Wagner DE, Bonvillain RW, Jensen T, Girard ED, Bunnell BA, Finck CM, Hoffman AM, Weiss DJ. Can stem cells be used to generate new lungs? *Ex vivo* lung bioengineering with decellularized whole lung scaffolds: Ex vivo lung bioengineering. Respirology 2013;18:895–911. [PubMed: 23614471]

56. Badylak SF, Taylor D, Uygun K. Whole-organ tissue engineering: Decellularization and recellularization of three-dimensional matrix scaffolds. Annu Rev Biomed Eng 2011;13:27–53. [PubMed: 21417722]

57. Singelyn JM, DeQuach JA, Seif-Naraghi SB, Littlefield RB, Schup-Magoffin PJ, Christman KL. Naturally derived myocardial matrix as an injectable scaffold for cardiac tissue engineering. Biomaterials 2009;30:5409–5416. [PubMed: 19608268]

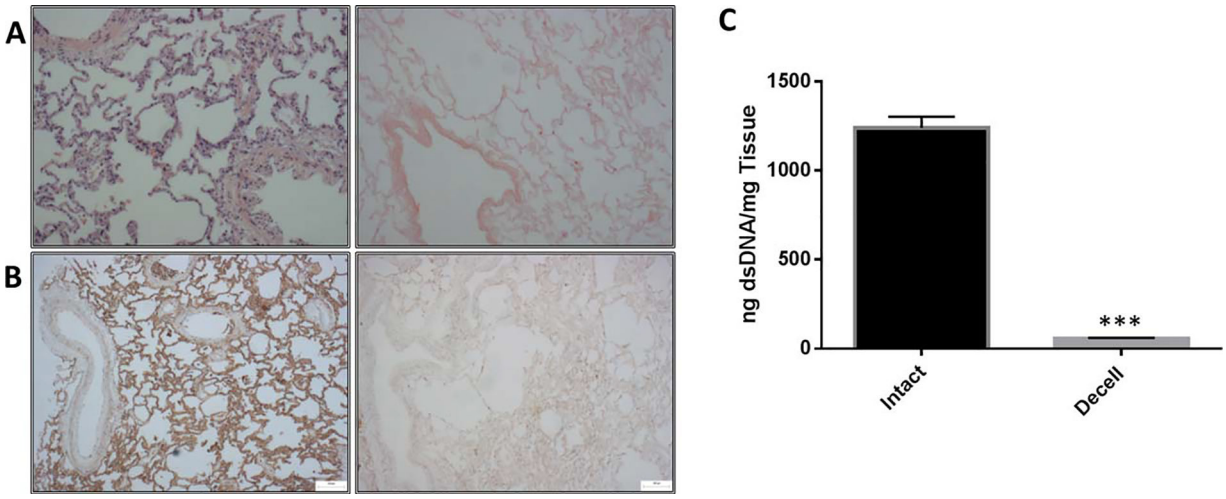

FIGURE 1.

Porcine Lung Tissue Decellularization. (A) H&E staining of porcine lung tissue fixed before and after decellularization indicating the removal of most nuclei, (B) α-galactosidase staining shows a reduction of the immunogenic alpha-gal membrane epitope, (C) dsDNA picogreen assay confirmed a 95.3% reduction in double stranded DNA. Data are mean +/− st.dev. $n = 3$ per group. *** $p < 0.001$ compared with the intact. Scale bars are 100 μm.

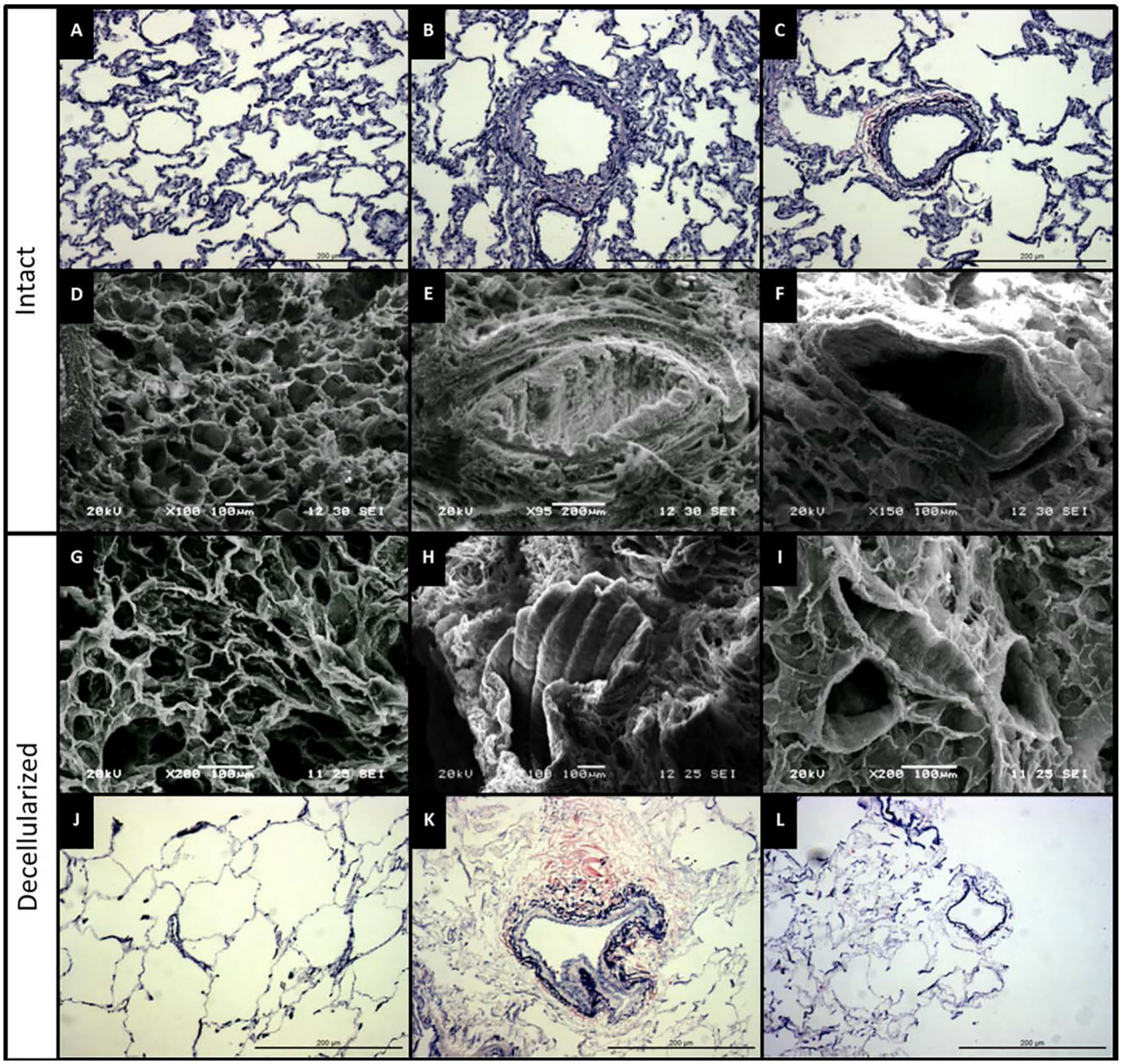

FIGURE 2.

Intact versus Decellularized Lung Tissue Comparison. SEM and Histology images from both intact (A–F) and a decellularized (G–L) lung slices comparing similar structures: first column (A,D,G,J) Alveolar Tissue; second column (B,E,H,K) airway structures; third Column (C,F,I,L) vasculature Structures. Histology samples stained using Accustain Elastic Stain: Black/Dark Purple: Elastic Fibers; Red/Pink: Collagen. Scale bars are 100 μm for SEM and 200 μm for light images.

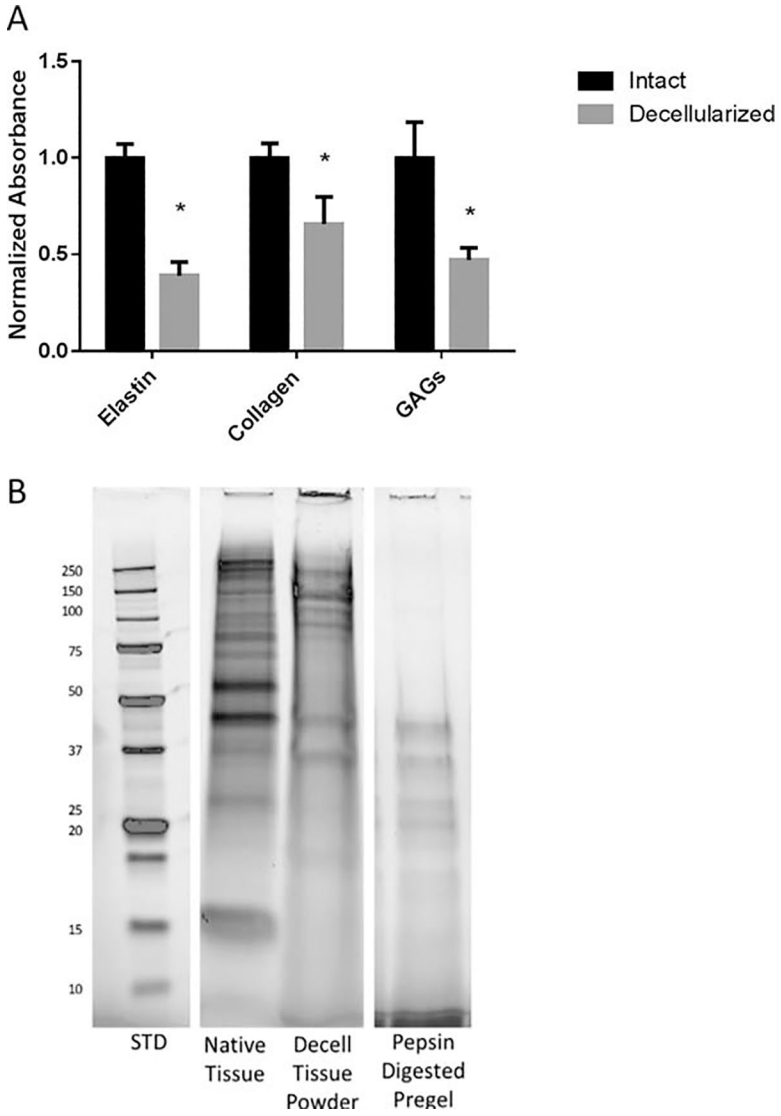

FIGURE 3.

Matrix Composition. (A) Quantification of major ECM components: elastin, collagen, and GAGs, showing the relative reduction caused by the decellularization process. Data are presented as mean +/− st.dev, $n = 3–4$ per group $p < 0.05$ as measured by t test. (B) SDS-PAGE gel shows how protein size and distribution change as tissue is processed to a powder and further digested into a pre-gel solution.

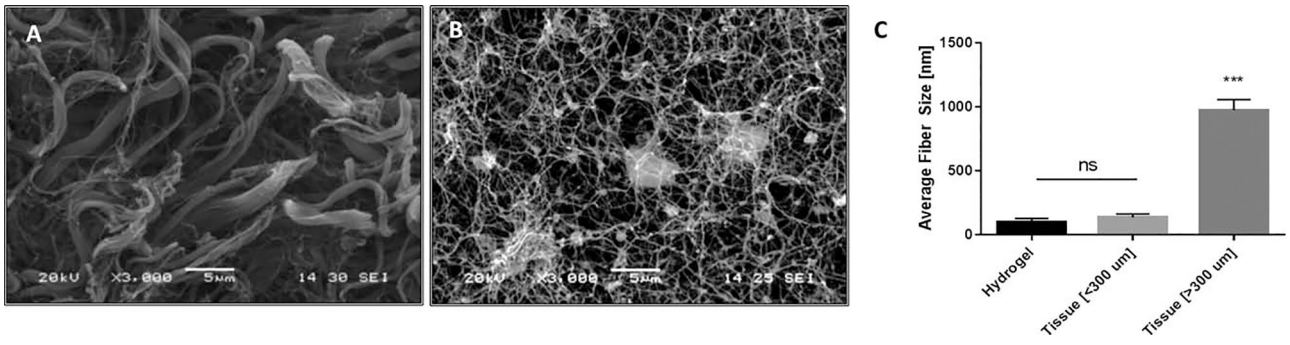

FIGURE 4.

Fiber Size Comparison: Decellularized Lung Tissue vs. Lung ECM Hydrogel. SEM of (A) pig lung tissue after decellularization and (B) a pig lung derived ECM hydrogel. (C) Quantification of average fiber size found in each set of samples, measured using Matlab image processing. While fiber bundles in the tissue samples are much larger, the small fibers (<300 nm) are more similar to those found in the hydrogel. *** $p < 0.0001$ for comparison to both the hydrogel and tissue small fiber size groups. $n = 3–5$ for all groups. SEM scale bars are 5 μm.

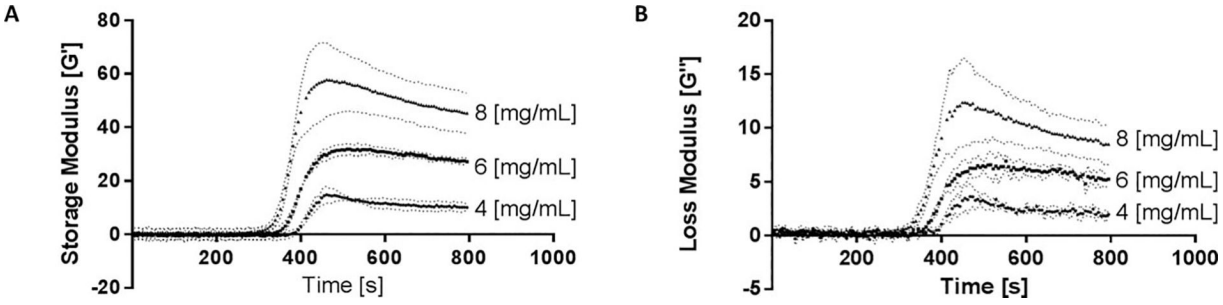

FIGURE 5.

Gelation Kinetics and Material Mechanics–Rheometry. (A) Storage modulus and (B) Loss modulus at the temperature is ramped from 4 to 37°C and then held constant. Rapid self-assembly takes place as the material approaches 37°C with the majority of gelation occurring within 3 min. Data are mean +/− st.dev. $n = 3$ per group.

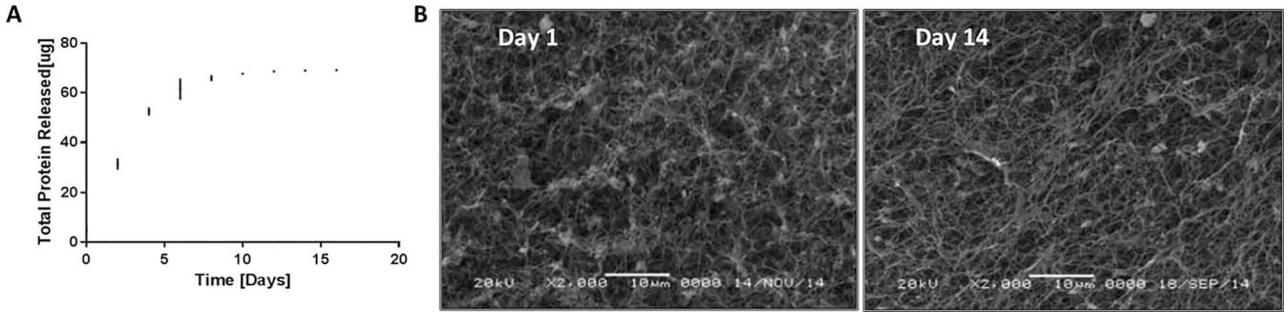

FIGURE 6.

Passive Release of protein from Hydrogels. (A) Protein release from hydrogels based on BCA Analysis of PBS supernatant, most protein loss occurs before day 8, data are mean +/− st.dev. $n = 3$ per group; (B) SEM comparison images from hydrogels fixed at day 1 compared with those fixed at day 14. Scale bars are 5 μm.

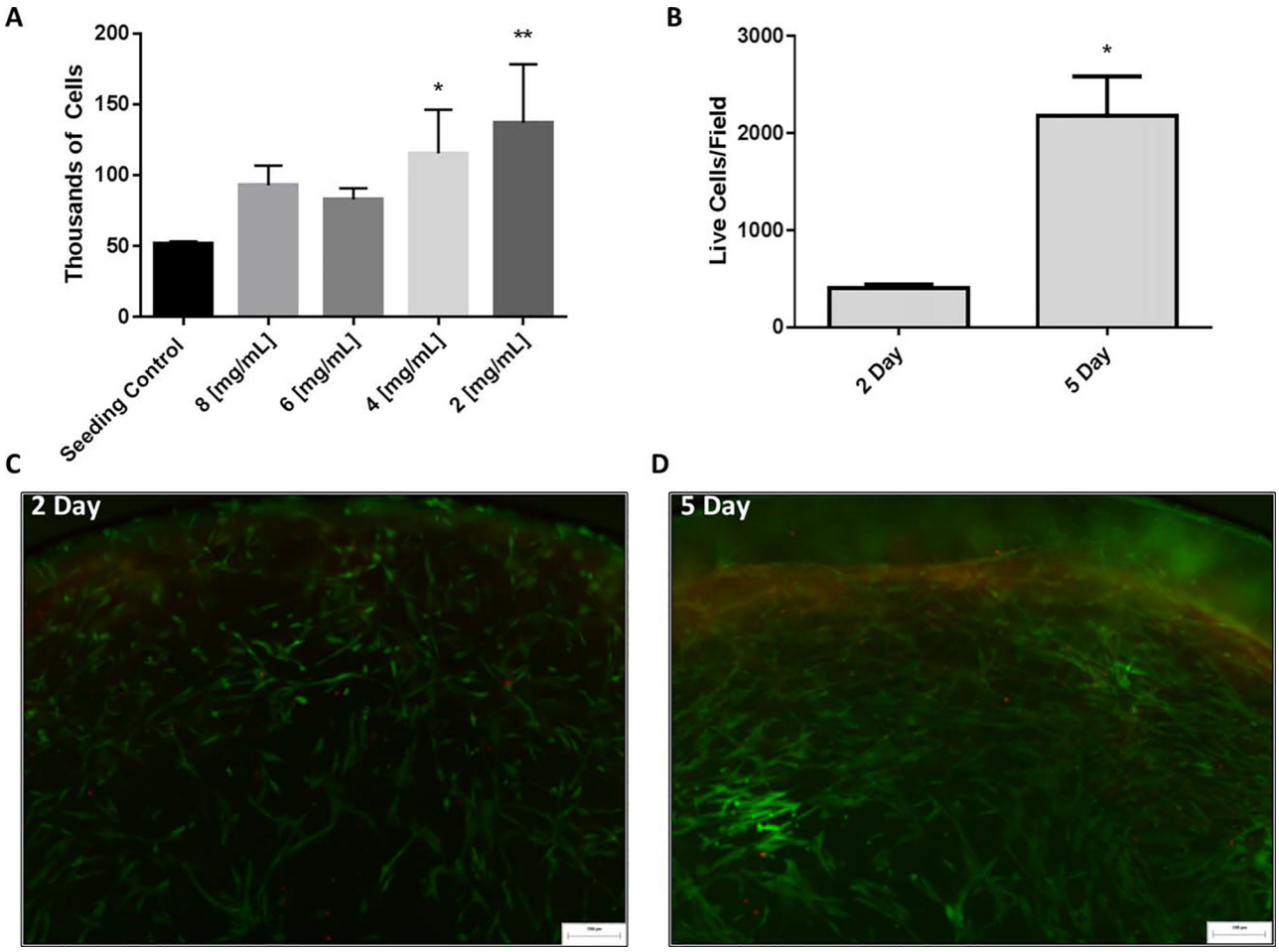

FIGURE 7.

Cell Viability Within Hydrogels. (A) 2 day encapsulated hMSC viability assay shows that cells remain viable following encapsulation. Data are mean +/− st.dev. $n = 3$ per group * $p < 0.05$, ** $p < 0.01$ compared with the seeding control; (B) Image analysis quantification of live/ dead assay. Live cells are reported as dead cells were negligible. Data are presented as mean +/− st.dev. $n = 3$ per group. *$p < 0.05$ comparing 2 and 5 days, indicating cell proliferation (C,D) Representative images from hMSCs encapsulated in lung ECM hydrogels and stained using a Live/Dead kit at 2 and 5 days of culture.

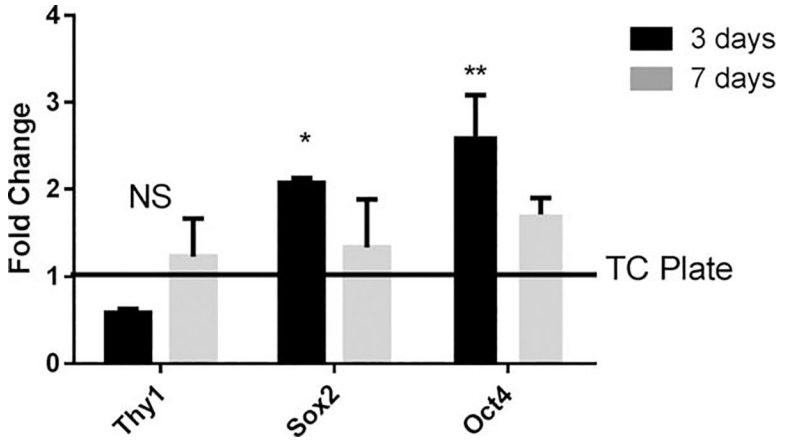

FIGURE 8.

Encapsulated hMSC Gene Expression. QPCR data from cells encapsulated in ECM hydrogels for 3 and 7 days and compared to a 3 day plate control. Gene expression indicates that both Sox2 and Oct4 are upregulated at 3 days of encapsulation but all three genes return close to their control levels by 7 days of encapsulation. Data are presented as mean +/− std. dev. $n = 3$ per group. $*p < 0.05$ compared with plate control.

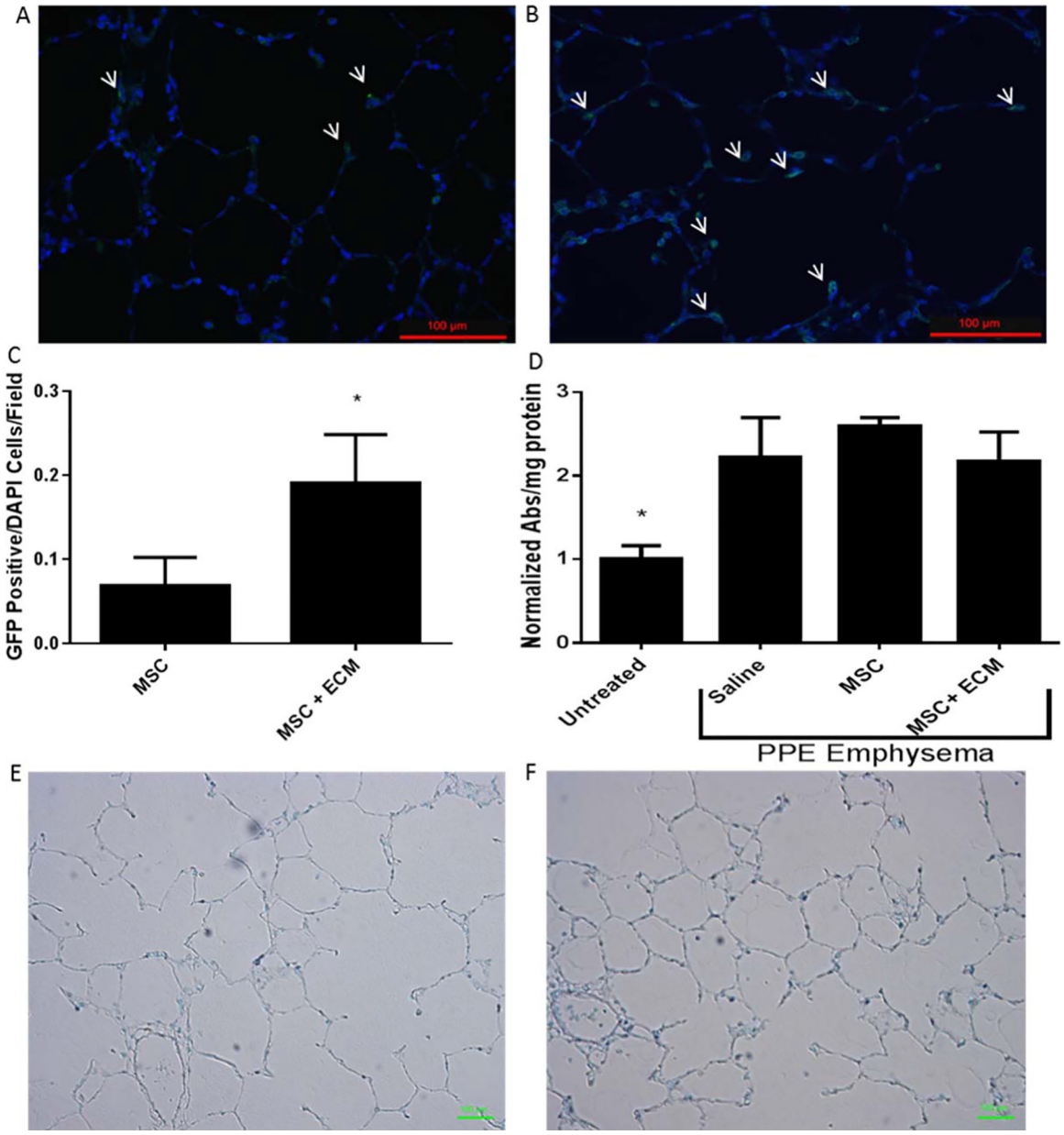

FIGURE 9.

Cell Deposition in Elastase Treated Rat Lungs. Cell deposition in elastase treated rat lungs. (A) Representative image from MSCs delivered in saline stained with anti-GFP to track the MSCs. (B) Representative image from MSCs delivered in ECM pre-gel solution stained with anti-GFP to track the MSCs. Arrows point to GFP+ cells. Scale bars are 100 μm. (C) Quantification of GFP positive rat MSCs per field in elastase treated rat lungs. Significantly greater numbers of GFP positive rat MSCs were present in the damaged lungs in the MSCs delivered in the ECM pre-gel solution compared with MSCs delivered in saline. Data are presented as mean +/− std. dev. $n = 3$ rats per group. Counts were from 10 fields/rat. $*p < 0.05$. (D) MPO assay of treated rat lungs. All elastase treated animals had significantly greater MPO activity compared with healthy animals. No statistical differences were

observed between treated groups, indicating that MSC and MSC + ECM do not cause any additional inflammatory response at 24 h. Data are presented as mean +/− std. dev. *$p <$ 0.05. (E,F) Representative apoptosis detection stained slides from MSC treated rats (E) and MSC + ECM treated rats (F). Sections stain with blue/green counterstain in all samples. No dark brown staining was observed, indicating a lack of apoptotic cells. Scale bars are 100 μm.

TABLE I.

Comparison to Similar Hydrogel Platforms

Material	Concentration	Storage Modulus (Pa)	SD	Reference
Lung	8 (mg/mL)	59.02	± 13.53	
	6 (mg/mL)	32.02	± 1.87	
	4 (mg/mL)	15.27	± 2.87	
Adipose	4–12 (mg/mL)	10–15		35
Cardiac	8 (mg/mL)	9.52	± 3.77	31
	6 (mg/mL)	5.28	± 0.41	
Dermis	8 (mg/mL)	466.5	± 64.3	
UBM	8 (mg/mL)	143.8, 182.2	± 84.1, ± 36.5	34,37
	4 (mg/mL)	11.43	± 4.9	
Brain	8 (mg/mL)	61.8	± 11	37
	4 (mg/mL)	20.3	± 16.0	
SC-ECM	8 (mg/mL)	757	± 74.9	37
	4 (mg/mL)	138.5	± 33.8	

Comparison of final storage modulus of Lung derived Hydrogels to published values for hydrogels derived from other ECM sources.